IMPROVED DIRECT ANALYSIS IN REAL TIME-MASS SPECTROMETRY SAMPLING FOR REPRODUCIBLE AND QUANTITATIVE ANALYSES

A Thesis
Presented to
The Academic Faculty

by

José Javier Pérez Jr.

In Partial Fulfillment
of the Requirements for the Degree
Master of Science in Chemistry in the
School of Chemistry and Biochemistry

Georgia Institute of Technology
August 2016

IMPROVED DIRECT ANALYSIS IN REAL TIME-MASS SPECTROMETRY SAMPLING FOR REPRODUCIBLE AND QUANTITATIVE ANALYSES

Approved by:

Dr. Facundo M. Fernández, Advisor
School of Chemistry and Biochemistry
Georgia Institute of Technology

Dr. Jiri Janata
School of Chemistry and Biochemistry
Georgia Institute of Technology

Dr. Cameron Sullards
School of Chemistry and Biochemistry
Georgia Institute of Technology

Date Approved: May 4, 2016

This thesis is dedicated to my wife, Angela Ann Pérez, and three daughters, Kaitlyn Belle Curiel, Aaliyah Renee Pérez, and Sarah Alexis Pérez, who each inspired me to succeed for them in their own unique and special ways. Their support and sacrifice throughout this journey is immeasurable.

ACKNOWLEDGEMENTS

Words could not possibly express the absolute sincere appreciation I have for those who both supported and sacrificed so much during my pursuit for my graduate research and education. I would first like to thank my advisor, Dr. Facundo Fernández, for his willingness to take me on as a part-time graduate student as I continued my full-time employment as a Research Chemist with the Centers for Disease Control and Prevention (CDC). As such, his patience, understanding, and frequent motivation to never let me quit went, what I feel to be, above and beyond expectation. I am forever grateful. I am also thankful for those within Dr. Fernandez's research group who assisted in my research endeavors: Dr. Christina Y. Hampton, Dr. Glenn A Harris, Dr. Christina M. Jones, Dr. María Eugenia Monge, Dr. Prabha Dwivedi, and Dr. Manshui Zhou. Additionally, I am grateful to my graduate committee and all others who worked with or alongside me.

None of this would have been possible if it not had been for those at the CDC who also provided supported. I am thankful for the opportunity provided to me by all levels of the supervisory chain who felt it worth their time and resources to support me during my time within the graduate program. I would specifically like to thank the late, Dr. Larry Needham, Dr. Dana Barr, Dr. Roberto Bravo Cárdenas, Dr. Clifford Watson, Dr. Benjamin Blount, and Dr. Liza Valentín-Blasini. Additionally, I am grateful to my many colleagues and personal and professional friends who took a personal interest in my advancement through this program.

And last, but certainly not least, I would like to express the greatest thanks to my family. No one sacrificed more than my wife, Angela Pérez, and three beautiful and amazing daughters, Kaitlyn Belle Curiel, and Aaliyah Renee and Sarah Alexis Pérez. As this journey comes to an end, I look forward to repaying them with all the love and affection they each so very much deserve. I, of course, would also like to thank my parents, José Javier Pérez Sr. and Rosie Valdez, Perez, for being so proud and supportive all the way through. I am thankful for the support and pride I received from my sisters Monica Annette Pérez, Erica Alejandra Lerma, and Kristina Elisa Pérez, as well as my nephews for seeing me as a role model and inspiring me to succeed for them as well.

TABLE OF CONTENTS

LIST OF TABLES

LIST OF FIGURES

LIST OF ABBREVIATIONS

2D	two-dimensional
3D	three-dimensional
APCI	atmospheric pressure chemical ionization
CE	capillary electrophoresis
CF	cystic fibrosis
CFD	computational fluid dynamic
CFRD	cystic fibrosis related diabetes
CID	collisional induced dissociation
CRM	consecutive reaction monitoring
DART	direct analysis in real time
DESI	desorption electrospray ionization
EBC	exhaled breath condensate
ESI	electrospray ionization
GC	gas chromatography
He*	excited-state helium
ITNs	insecticide-treated nets
LC	liquid chromatography
LIT	linear ion trap
LLINs	long-lasting insecticidal nets
LOD	limit of detection
MS	mass spectrometry
MS/MS	tandem mass spectrometry

PEG	poly(ethylene glycol)
QqQ	triple quadrupole
TLC	thin layer chromatography
TM-DART	transmission-mode direct analysis in real time
TM-DESI	transmission-mode desorption electrospray ionization
TOF	time-of-flight
TWIMS	traveling wave ion mobility spectrometry
UHPLC	ultra-high performance liquid chromatography
WHO	World Health Organization

SUMMARY

Transmission-mode direct analysis in real time (TM-DART) is presented as an alternative sampling strategy to traditional methods of sample introduction for DART MS analysis. A custom-designed sample holder was fabricated to rapidly and reproducibly position insecticide-treated nets normal to the ionizing metastable gas stream, enabling transmission of desorbed analyte ions through the holder cavity and into the MS. Introduction of the sample at this fixed geometry eliminates the need for optimizing sample position and allows spectra based on factors such as metastable gas temperature and flow to be systematically evaluated. The results presented here, supported by computational fluid dynamic simulations, demonstrate the effects of these factors on the resulting mass spectra and the potential of this sampling strategy to be used for qualitative and quantitative analyses. Transmission-mode desorption electrospray ionization (TM-DESI) experiments on similar insecticide-treated nets were performed for comparison purposes.

CHAPTER 1

INTRODUCTION

The following chapters describe research conducted by multiple persons; the contents of which were adapted with permission from the resulting published work.[1] J.J. Pérez conducted all TM-DART-MS experiments. G.A. Harris performed finite element simulation experiments for TM-DART-MS configurations. All TM-DESI-MS experiments were conducted, via collaboration with the University of Texas at Austin, by J.E. Chipuk under J.S. Brodbelt.

The introduction of desorption electrospray ionization (DESI) in 2004[2] and direct analysis in real time (DART) in 2005[3] led to the inception of the continuously growing sub-field of ambient desorption ionization techniques in mass spectrometry (MS). Ambient desorption ionization allows direct, rapid, high-throughput analyses of virtually any sample surface under ambient conditions minimizing, if not altogether eliminating, the need for sample manipulation or preparation steps. This modern-day field has since seen a plethora of new ionization techniques developed,[4-9] each with their own unique acronym, seeking to improve the sensitivity and selectivity of rapidly probing samples of virtually any size or shape in the open air. Depending on the technique, analyte surface desorption and ionization processes occur either separately or simultaneously by some focused external form of energy under ambient conditions, where it is then subject to mass analysis.

DART allows for rapid sample analysis by introducing the sample within the ionization region between the gas outlet of the DART source and the inlet orifice of the mass spectrometer.[3, 10] DART is an atmospheric pressure chemical ionization (APCI)-type ambient ionization source consisting of a point-to-plane glow discharge housed

within the source compartment. A plasma containing electrons, excited-state helium (He*) atoms (metastables), and other charged species is produced by this discharge at approximately 3600 V and heated upwards of 500 °C before exiting the source. Nitrogen gas may also be used in place of helium as the discharge gas, however, is much less frequently used. Perforated grid electrodes filter out charged species to prevent ion-ion and ion-electron recombination, resulting in only neutral metastables and gas atoms or molecules to exit the ion source. This heated gas stream partially acts to induce thermal desorption of analytes from a given sample surface or substrate placed with the ionization region. Within the DART ionization region, metastable He* atoms generate positive ions *via* several proposed mechanisms. The first involves the production of protonated water cluster ions *via* Penning ionization of atmospheric water molecules by metastable helium atoms (Eq. 1).[3]

$$He^*(g) + nH_2O(g) \longrightarrow He(g) + (H_2O)_{n-1}H^+(g) + OH^-(g) \qquad \text{(Eq. 1)}$$

Proton-transfer reactions between cluster ions and thermally-desorbed analyte molecules (M) (Eq. 2a) from solid and liquid samples produce protonated analyte ions (Eq. 2b).[11]

$$M(s) \xrightarrow{heat} M(g) \qquad \text{(Eq. 2a)}$$

$$M(g) \xrightarrow{(H_2O)_{n-1}H^+(g)} M(H_2O)_{n-2}H^+(g) + H_2O(g) \xrightarrow{-(n-2)H_2O} MH^+(g) \qquad \text{(Eq. 2b)}$$

Another mechanism suggests direct Penning ionization[12] of analytes to produce positive molecular ions ($[M]^{+\bullet}$).

$$He^*(g) + M(g) \longrightarrow He(g) + M^{+\bullet}(g) + e^- \qquad \text{(Eq. 3)}$$

Production of the $[M]^{+\bullet}$ for low polarity analytes *via* charge-exchange reactions with oxygen molecular ions ($[O_2]^{+\bullet}$) has also been reported (Eq. 4a and 4b).[11]

$$He^*(g) + O_2(g) \longrightarrow He(g) + O_2^{+\bullet}(g) + e^- \qquad \text{(Eq. 4a)}$$

$$O_2^{+\bullet}(g) + M(g) \longrightarrow O_2(g) + M^{+\bullet}(g) \qquad \text{(Eq. 4b)}$$

These mechanisms, however, will only prevail if the ionization energy of the analyte is lower than the internal energy of the metastable species (19.8 eV for the 2^3S_1 state of helium) or of $[O_2]^{+\bullet}$ (12.07 eV). Negative ionization mechanisms investigated in DART[13] have been attributed to four possible pathways including electron capture (negative molecular ion; $[M]^{-\bullet}$), dissociative electron capture (fragment ions), proton transfer/abstraction ($[M - H]^-$), and anion/halide attachment (adducts). In DESI, ions are produced by directing charged solvent droplets from an electrospray source toward a surface. Analytes present at the surface are solvated by the electrospray to form an initial solvent layer; dislodged by the momentum transferred by the impact of secondary droplets; and ultimately ionized by typical electrospray mechanisms.[8, 14] For both DART and DESI, the resulting gas-phase ions are transferred to the mass spectrometer inlet orifice by the continuous gas or solvent flows, the influence of the applied potential, and the pressure differential between the ionization region and the spectrometer's interface.

The number and types of applications have evolved tremendously since DART was first introduced.[10] Initial applications focused largely on its rapid screening capabilities to directly ionize and qualitatively analyze low molecular weight molecules in or on simple solid, liquid, and gaseous samples or sample surfaces. Such early applications included pharmaceutical[15, 16] and counterfeit[17-20] drug analysis; trace analysis of explosives, warfare agents, or illicit drugs on luggage, clothing, or bank notes;[3, 13, 21, 22] readout of TLC plates in planar chromatography,[23] characterization of self-assembled monolayers on gold surfaces,[24] flavors and fragrances,[25] and forensic analysis.[26-33] DART-MS applications rapidly evolved towards the analysis of more complex biological

matrices enabling fatty acid profiling of whole bacterial cells[34] and targeted and untargeted metabolomics approaches in urine and blood matrices.[35-39] Semi-quantitative[40, 41] and quantitative[21, 42-44] methods have also been realized using DART-MS methods. The DART analysis of a macroscopic object's surface (e.g. drug tablets, TLC plates, etc.) requires the sample to be held in a position which allows for the reactive DART gas stream to flow tangentially to the surface, and avoid blocking the flow of desorbed analyte ions into the MS.[45] Liquids are commonly analyzed by first dipping the end of a melting point tube into the sample and then holding it within the ionizing gas stream, which causes rapid drying and ionization. Coupling of DART with separation techniques including gas chromatography (GC),[11] liquid chromatography (LC),[46] and capillary electrophoresis (CE)[47] is also possible by guiding the eluent into the ionization region. Commercial versions of the DART ion source also allow the angle of the incident metastable gas stream to be adjusted for optimization.[48] The focus of this research was to develop a transmission-mode DART (TM-DART)[1] methodology as an alternative sampling strategy for DART MS. The work presented here introduces the first TM-DART sampling strategy using a mesh sample as a proof-of-principle application. Qualitative and quantitative TM-DART MS analyses of insecticide-treated nets (ITNs), i.e. bednets, coated with pyrethroid pesticides are shown as examples of the types of application that can benefit from this approach. ITNs are widely used in control and prevention of malaria transmission in endemic countries, and are a central component of national malaria programs. A custom-designed sample holder was fabricated to rapidly and reproducibly place the bednets normal to the ionizing metastable gas stream. Three-dimensional finite element simulations of the fluid dynamic properties of the sampling

region were performed to investigate the effect of this sample holder on the fluid dynamics within the ionization region. For comparison purposes, TM-DESI[49] was also performed on identical bednet samples.

CHAPTER 2

EXPERIMENTAL

2.1 Chemicals and Materials

Pure deltamethrin (99%) and permethrin (20% *cis*; 78% *trans*) standards were obtained from Chem Service (West Chester, PA). Poly(ethylene glycol) (PEG 600) was obtained from Sigma-Aldrich (St. Louis, MO) and used as mass calibration standard. High-purity He and N_2 (99.999%) gases used in DART experiments were obtained from Airgas, Inc. (Atlanta, GA). Conventionally-treated nets coated with varying levels of deltamethrin (0.5, 1, 2, 4, 8, 16, and 55 mg m^{-2}) were prepared by dipping blank polyester nets into aqueous formulations of varying concentrations of the insecticide. After all the insecticide solution was soaked, the treated net was laid out flat to dry. Long-lasting insecticidal nets (LLINs) PermaNet® 2.0 and Olyset® were obtained from Vestergaard-Frandsen (Denmark) and Sumitomo Chemical Co. Ltd., respectively.

2.2 Transmission-mode sample holders

For the TM-DART analyses, a custom-made sample holder was fabricated in-house (Figure 2.1). Bednet sections were sandwiched between two 57 mm × 3.2 mm × 19 mm MACOR slides each containing a centered 5 mm diameter hole. This assembly was placed onto an aluminum holder and mounted in between the DART ion source gas outlet and the mass spectrometer inlet orifice, exposing a 20 mm^2 bednet area to the metastable gas stream. Notches in the sides of the aluminum sample holder allowed for it to easily

be slid on and off custom-made screws mounted into pre-threaded holes of the DART ion source. This design provided reproducible, quick, and easy mounting/dismounting of the sample/holder assembly to a fixed position within the ionization region.

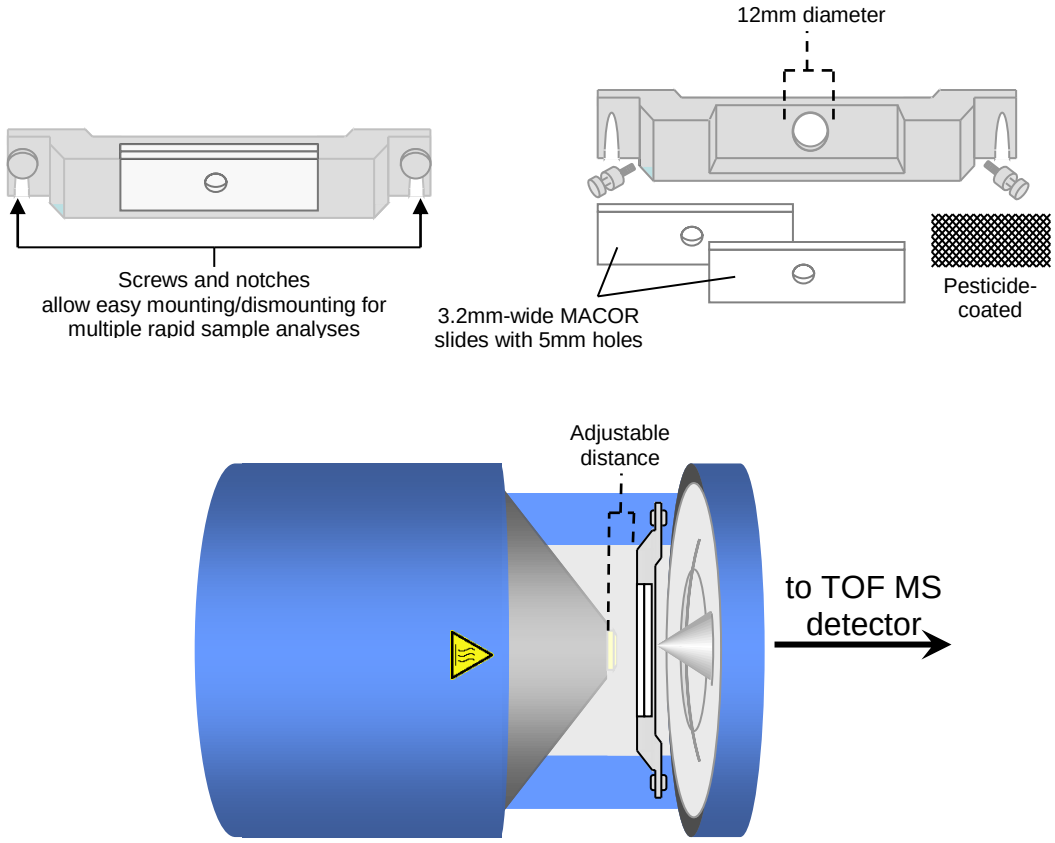

Figure 2.1. Schematics of the custom-made sample holder used for TM-DART analysis. Upper-left view displays the assembled sample holder; upper-right view displays an exploded view of the sample holder; bottom view illustrates a top-view of the sample holder assembly mounted in the ionization region of the TM-DART TOF mass spectrometer interface.

For TM-DESI analyses, a prototype adaptor kit was manufactured by Prosolia Inc. (Indianapolis, IN) and used to convert a standard Omni Spray® 1-D scanning source to a customized source more suitable for TM-DESI. The adaption included a slotted sample holder in place of the conventional slide holder and the use of custom-sized TM-DESI mesh holders. Bednets were held in place by affixing them to a 26 mm × 76 mm × 3 mm

PEEK backing plate with an 8 mm × 38 mm slot cut into it to facilitate transmission of the electrospray through both the sample and the backing plate. In addition, experiments were also conducted where a sample mask with 4 mm square cutouts was placed over the backing plate and sample, thereby isolating the mesh between the backing plate and the mask, and creating six equal 4 mm × 4 mm subsamples.

2.3 Transmission-mode DART TOF MS

A DART ion source (IonSense, Danvers, MA) coupled to a JMS-T100LC (AccuTOF™) orthogonal time-of-flight mass spectrometer (TOF MS, JEOL, USA, Peabody, MA) was used for high-accuracy mass measurement experiments performed in positive ion mode using either He or N_2 gas. The flow rate of He gas was varied between 0.55 and 2.0 L min^{-1} to determine its effect on the resulting spectra. The flow rate of N_2 gas was held at 7.0 L min^{-1}, as lower flow rates did not produce a stable and reproducible baseline signal. Therefore, the effect of varying the N_2 gas flow could not be evaluated. The distance between the exit of the DART ion source and the sample holder was examined at two positions: (A) in contact with one another, and (B) 4 mm apart. These distances were used to compare the spectra obtained from varying gas flow rates. The gas heater temperature was varied between 100 °C and 225 °C to determine the effects of temperature on the resulting spectra. The glow discharge needle voltage of the DART source was set to 3500 V and the discharge and grid electrode voltages were 150 V and 250 V, respectively. The TOF mass spectrometer ion optics settings were as follows: inlet orifice voltage: 20 V for He-DART and 30 V for N_2-DART; ring electrode voltage: 5 V; orifice 2: 5 V; ion guide bias voltage: 29 V; ion guide peaks voltage: 300 V for He-DART and 500 V for N_2-DART. The detector voltage was set to 2750 V. Mass

calibration was performed by placing a 1.5 mm o.d. × 90 mm long glass capillary tube dipped in a concentrated PEG solution in the metastable gas stream for 30 s and obtaining a reference mass spectrum. Mass spectral data acquisition, processing, calibration, and background subtraction were performed using the built-in mass spectrometer software, MassCenter 1.3.

2.4 Transmission-mode DESI MS

The Prosolia Omni Spray® ion source was mounted to a Thermo Fisher Scientific LTQ XL mass spectrometer (Thermo Fisher Scientific Inc., Waltham, MA) and modified to allow a zero-degree angle between the electrospray tip and capillary inlet. Mass spectra were acquired by scanning the sample at a rate of 250 mm s^{-1}. For all analyses the distance between the electrospray tip and the sample was 2 mm, while the distance between the sample and the capillary inlet was 6 mm. Mass spectra were acquired using the Xcalibur 2.0 software program in positive ion mode, with the ion accumulation time set to 10 ms, and signal averaging set for 3 microscans. The integrated syringe pump of the LTQ XL was used to deliver a solution of acetonitrile (90%), water (10%), and ammonium acetate (10 mM) at a rate of 5 mL min^{-1} as the electrospray solvent. The electrospray voltage was set to +4 kV. Nitrogen at a pressure of 110 psi was used as the electrospray nebulizing gas and the temperature of the heated capillary was held at 150 °C.

2.5 Finite element simulations

A three-dimensional design geometry file was created depicting the accurate dimensions of the DART gas exit nozzle, sample holder and MS inlet orifice with the

computer-aided design program within the COMSOL Multiphysics® (COMSOL, Inc., Burlington, MA, USA) finite element analysis environment. The modeled flow rates, gases, and sample holder spacing matched those used in the DART experiments. All models were built in the absence of electric fields and without regard to the influence of reduced pressure transport originating at the inlet of the mass spectrometer. Transient (200 ms) simulations were performed on a dual Intel Xeon quad core (2.66 GHz) computer with 8 GB memory and 1.5 GB video memory. Simulations required between 0.75 and 12.5 h to complete depending on the chosen conditions, with higher flow rates requiring longer due to the increased complexity of the fluid dynamics.

CHAPTER 3

RESULTS AND DISCUSSION

Bednets treated with insecticides, such as the pyrethroids deltamethrin and permethrin, have been shown to significantly reduce the morbidity and mortality rates associated with malaria.[50-52] Conventionally-treated nets are prepared by dipping polyester meshes into a pyrethroid water emulsion and allowed to dry, leaving a relatively uniform residue of insecticide on their surface. Because the efficacy of conventionally-treated nets is reduced due to loss of the insecticide from environmental exposure and repeated washing,[53] methods for impregnating insecticides into nets have been developed, leading to long-lasting insecticidal nets (LLINs) of various types.[54] LLINs maintain a slow release and migration of the insecticide toward the surface of the net, resulting in much improved wash resistance. The amount of insecticide on bednets can be assessed by direct laboratory methods based on gas or liquid chromatography, direct field colorimetric methods, or indirect bioassays, such as the World Health Organization (WHO) Cone Test.[55] The presence of the insecticide on the surface and the open mesh structure of ITNs make them also amenable to surface analysis by TM-DESI[49] and TM-DART MS, as demonstrated below. He- and N_2-induced DART TOF MS spectra of neat deltamethrin (Figure 3.1) and

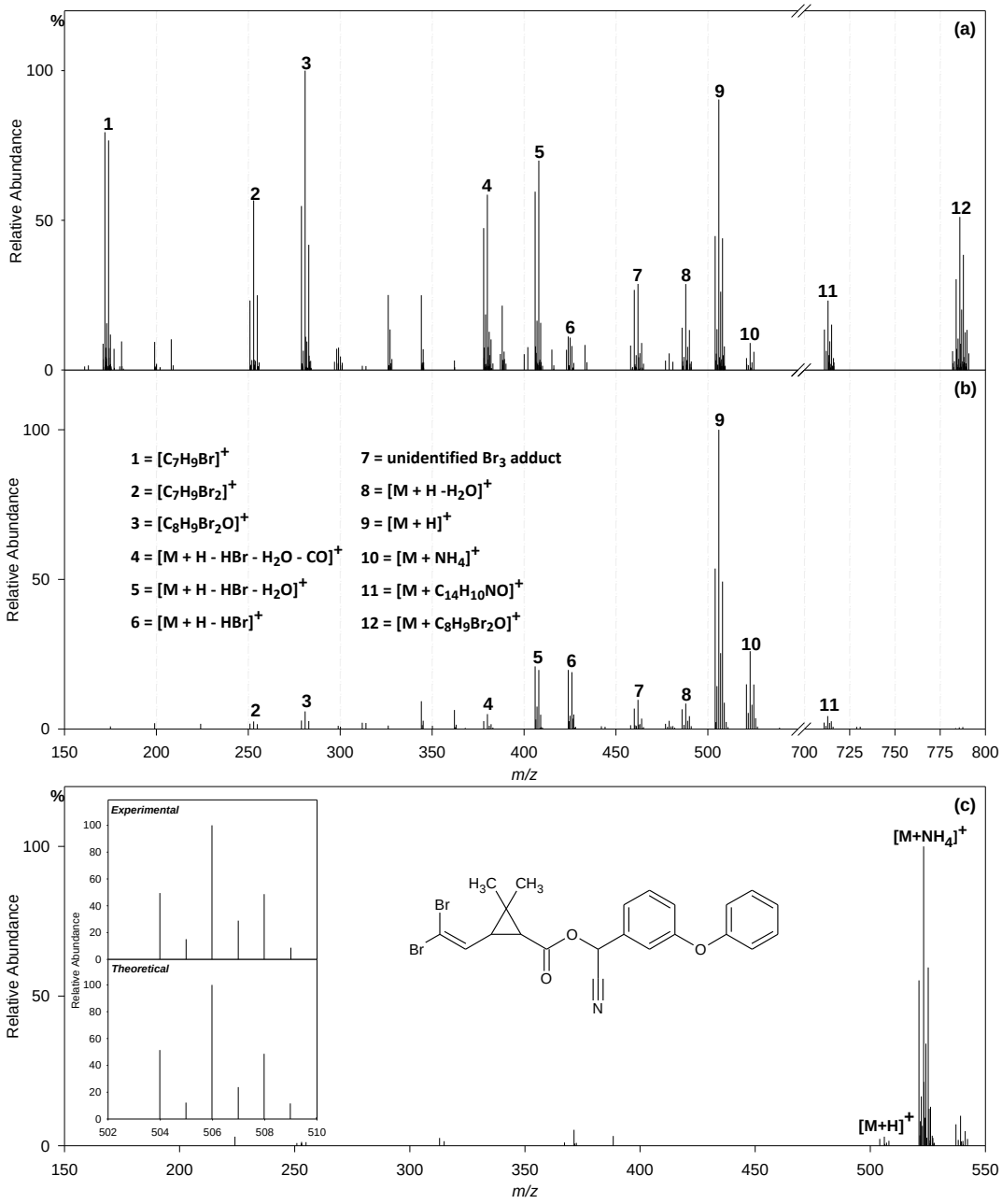

Figure 3.1. He-induced DART TOF MS spectra of a neat deltamethrin standard obtained at (a) 225 °C and (b) 150 °C with 1.5 L min^{-1} gas flow rate. Fragmentation was observed when helium was used as the ionizing gas, increasing with temperature. The N_2-induced spectrum shown in (c) represents a predominant $[M + NH_4]^+$ ion with little-to-no fragmentation (225 °C, 7.0 L min^{-1}). The insets in panel (c) show the experimental and theoretical isotopic structures of the deltamethrin $[M + H]^+$ ion observed in the He-induced spectra. Spectral peak assignments and mass accuracies are listed in Table 3.1.

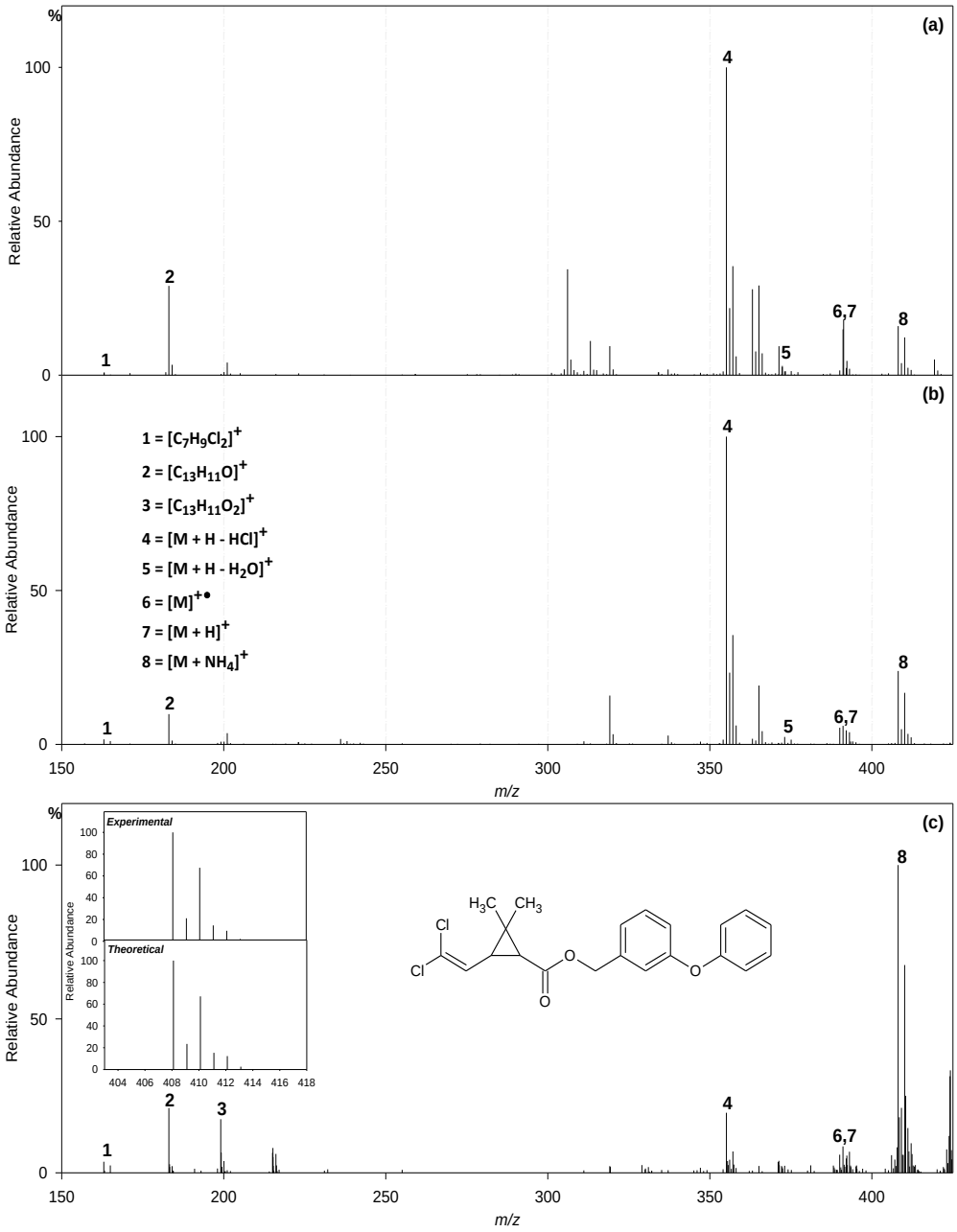

Figure 3.2. He-induced DART-TOF MS spectra of a neat permethrin standard obtained at (a) 225 °C and (b) 150 °C with 1.5 L min^{-1} gas flow rate. Significant fragmentation was observed when He was used as the ionizing gas, increasing only slightly with increasing temperature. The N_2-induced (225 °C, 7.0 L min^{-1}) mass spectrum (c) resulted in an abundant $[M+NH_4]^+$ ion but also considerable fragmentation compared to that of deltamethrin (see Figure 2.2). Insets in panel (c) show the chemical and isotopic (experimental and theoretical) structures of the permethrin pesticide. The inset showing the isotopic distribution corresponds to the $[M+NH_4]^+$ ion of the nitrogen-induced spectra. Spectral peak assignments and mass accuracies are listed in Table 3.2.

permethrin (Figure 3.2) standards deposited on a melting point capillary were obtained in positive ion mode to first identify mass spectral peaks specific to these pyrethroid insecticides. The chemical formulas, theoretical and experimental masses, and mass accuracies of diagnostic ions identified are listed in Tables 3.1 and 3.2.

Table 3.1. Identified peaks in the DART TOF MS helium spectrum of a neat deltamethrin standard.

Peak	Formula	Theoretical Mass	Experimental Mass	Δm (mmu)
1	$[C_7H_9Br]^+$	171.9882	171.9918	3.6
		173.9862	173.9872	1.0
2	$[C_7H_9Br_2]^+$	250.9066	250.9106	4.0
		252.9045	252.9079	3.4
		254.9025	254.9037	1.2
3	$[C_8H_9Br_2O]^+$	278.9015	278.9054	3.9
		280.8994	280.9025	3.1
		282.8974	282.8968	0.6
4	$[M+H-HBr-H_2O-CO]^+$	378.0488	378.0453	3.5
		380.0468	380.0489	2.1
5	$[M+H-HBr-H_2O]^+$	406.0437	406.0435	0.2
		408.0417	408.0367	5.0
6	$[M+H-HBr]^+$	424.0543	424.0488	5.5
		426.0522	426.0492	3.0
8	$[M+H-H_2O]^+$	485.9699	485.9673	2.6
		487.9678	487.9657	2.1
		489.9658	489.9683	2.5
9	$[M+H]^+$	503.9804	503.9822	1.8
		505.9784	505.9777	0.7
		507.9764	507.9771	0.7
10	$[M+NH_4]^+$	521.0070	521.0088	1.8
		523.0049	523.0107	5.8
		525.0029	525.0165	13.6
11	$[M+C_{14}H_{10}NO]^+$	711.0489	711.0469	2.0
		713.0468	713.0551	8.3
		715.0448	715.0661	21.3
12	$[M+C_8H_9Br_2O]^+$	781.8746	781.8784	3.8
		783.8726	783.8522	20.4
		785.8705	785.8613	9.2
		787.8685	787.8565	12.0
		789.8664	789.8708	4.4

Table 3.2. Identified peaks in the DART-TOF MS spectra of the permethrin standard.

Peak	Formula	Theoretical Mass	Experimental Mass	Δm (mmu)
		163.0076	163.0131	5.5
1	$[C_7H_9Cl_2]^+$	165.0046	165.0107	6.1
		167.0017	167.0020	0.3
2	$[C_{13}H_{11}O]^+$	183.0804	183.0809	0.4
3	$[C_{13}H_{11}O_2]^+$	199.0754	199.0761	0.8
4	$[M+H-HCl]^+$	355.1095	355.1097	0.2
		357.1066	357.1080	1.4
		373.0757	373.0798	4.1
5	$[M+H-H_2O]^+$	375.0727	375.0845	11.8
		377.0698	377.0828	13.0
		391.0862	391.0865	0.3
6	$[M+H]^+$	393.0833	393.0855	2.3
		395.0803	395.0911	10.8
		390.0784	390.0842	5.8
7	$[M]^{+\bullet}$	392.0755	392.0866	11.1
		394.0725	394.0872	14.7
		408.1128	408.1126	0.1
8	$[M+NH_4]^+$	410.1098	410.1107	0.9
		412.1069	412.1149	8.1

Figure 3.1a and b and 3.2a and b show He-DART TOF MS spectra of neat deltamethrin and permethrin standards, respectively, at (a) 225 °C and (b) 150 °C at a flow rate of 1.5 L min^{-1}. Figure 3.1c and 3.2c show N_2-DART TOF MS spectra for both insecticides obtained at 225 °C and 7.0 L min^{-1}. In the case of deltamethrin, it was observed that He yielded a higher abundance of the protonated molecule (peak 9) at 150 °C, while producing less fragmentation in comparison to 225 °C. Also, intense signals pertaining to mono- (peak 1) and dibrominated (peak 2) fragment ions arising from α-cleavage at the carbonyl group, ester bond cleavage (peak 3), and multiple neutral losses (peaks 4, 5, 6 and 8) were observed at 225 °C. In addition, adducts of thermally-induced fragment ions with neutral precursor molecules were observed. Peaks 11 and 12 corresponded to neutral deltamethrin molecules adducted with the cyano-containing benzyl cation $[C_{14}H_{10}NO]^+$, and the doubly brominated $[C_8H_9Br_2O]^+$ cation, respectively. Conversely,

N_2-DART performed at 225 °C resulted in low intensities of fragment ions and protonated molecules. Instead, the base peak was the ammonium adduct ion (peak 10) as commonly observed for carbonyl-containing compounds.[11] The presence of bromine atoms in the deltamethrin molecule yielded characteristic one- or two-Br isotopic patterns, which aided in the identification of ionic species. As an example, the inset in Fig. 3.1c shows the experimental isotopic distribution of the protonated deltamethrin monomer, which was consistent with the expected theoretical distribution. The He-DART analysis of permethrin yielded fewer fragment ions which only slightly increased in abundance when increasing the gas temperature from 150 °C to 225 °C (Figure 3.2a and b). The identities of the permethrin fragment and adduct ions were similar to some of those identified for deltamethrin, but with some interesting differences. The ions observed for He experiments were a result of α-cleavage at the carbonyl group (peak 1), cleavage to produce $[C_{13}H_{11}O]^+$ benzyl cations (peak 2), ester bond cleavage (peak 3), HCl and H_2O losses from the protonated molecule (peaks 4 and 5, respectively), and the intact protonated (peak 7) and ammoniated (peak 8) adduct ions. Interestingly, the permethrin $[M]^{+\bullet}$ molecular ion (peak 6) was observed, which was not the case for deltamethrin. The absence of a cyano functional group in permethrin resulted in a lower abundance of its protonated molecule (peak 7) when compared to deltamethrin, possibly due to the less localized nature of the positive charge in the $[M+ H]^+$ ion. In this case, the base peak corresponded to the HCl neutral loss (peak 4). He-DART TOF MS analysis of cypermethrin, the chlorinated analog of deltamethrin, showed the same relative fragment and adduct ion intensities as deltamethrin, reinforcing the notion of a stabilization effect driven by the cyano moiety (data not shown). The permethrin ammonium adduct (peak 8)

was the base peak in the N_2 spectrum (Fig. 3.2c), with only a small relative amount of fragment ions present. The lower-energy of N_2 metastables and the lower thermal conductivity of N_2 are believed to cause the reduced fragmentation observed in N_2. Interestingly, the absence of a charge-stabilizing cyano group caused a relatively larger degree of fragmentation in the N_2 spectrum of permethrin when compared to deltamethrin. Chlorine atoms present in permethrin were responsible for the characteristic one or two Cl isotopic patterns, shown in the inset in Figure 3.2c.

Figure 3.3 shows temperature-dependent TM-DART TOF MS spectra of conventionally-treated bednet sections coated with 55 mg deltamethrin m^{-2}.

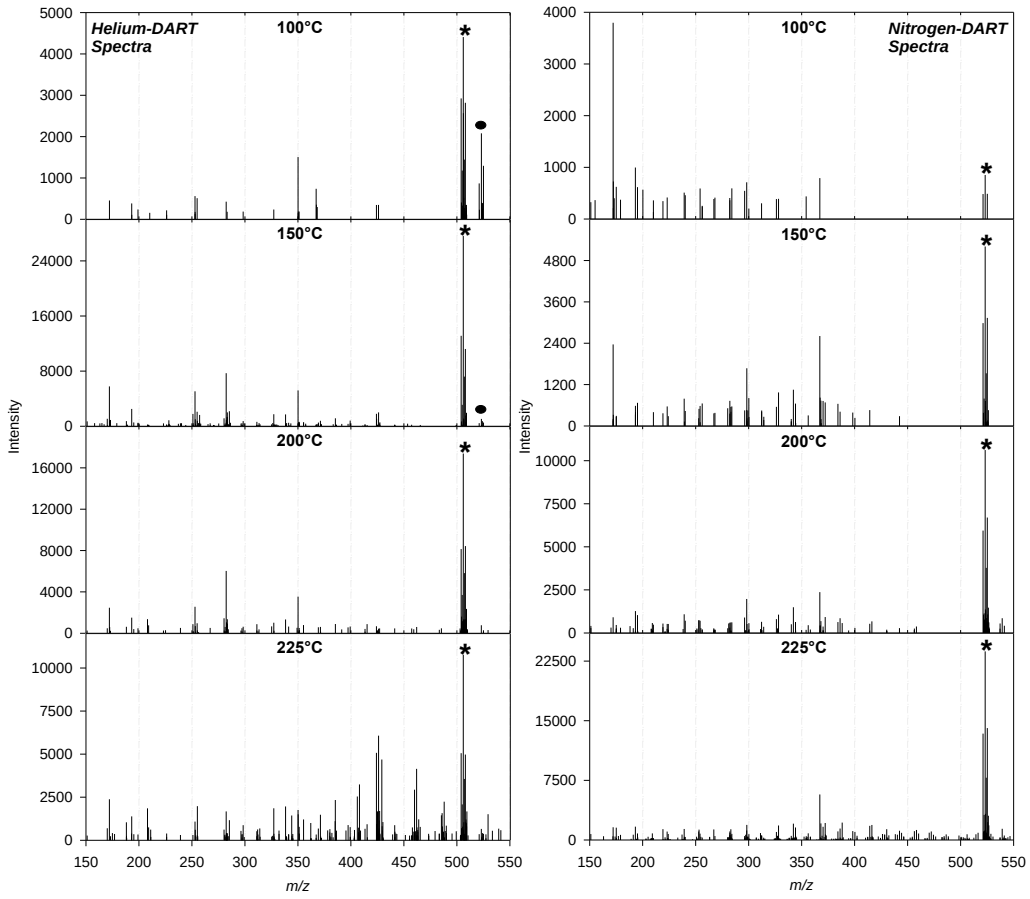

Figure 3.3. Impact of ionizing gas temperature on the resulting TM-DART TOF mass spectra. The effect of temperature was tested on a conventionally-treated bednet coated

with 55 mg deltamethrin m^{-2} with He (left column) and N_2 (right column) as the DART discharge gases. The $[M + H]^+$ and $[M + NH_4]^+$ ions are labeled (*) and (●), respectively.

The left and right columns show the effect of increasing the He and N_2 metastable gas stream temperature, respectively. In the He TM-DART spectra (Fig. 3.3, left column), an increase in temperature from 100 °C to 150 °C resulted in a marked increase in the $[M + H]^+$ ion absolute intensity and a decrease in the ammonium adduct intensity. This was due to increased abundance of background water cluster reagent ions at 150 °C. As the temperature of the He gas was further increased, the $[M + H]^+$ ion intensity began to decline due to increased thermal-induced fragmentation. When N_2 was used to support the DART glow discharge (Fig. 3.3, right column), a continuous increase in the $[M + NH_4]^+$ ion intensity was observed due to improved thermal desorption.

As indicated in Figure 2.1, the current sample holder and DART ion source configuration allow for the distance between the DART gas outlet and the bednet to be adjusted. Plots of the absolute intensity of the most abundant $[M + H]^+$ isotope ion at four different flow rates and two different sample positions are shown in Figure 3.4.

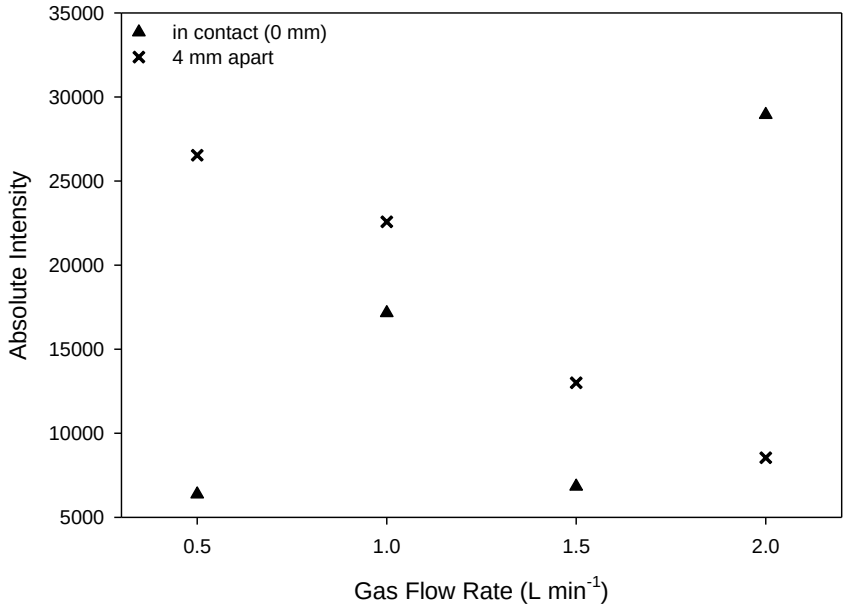

Figure 3.4. Effect of He gas flow rate on the absolute intensity of the most abundant $[M + H]^+$ isotope ion of deltamethrin during TM-DART analysis of a 55 mg m^{-2} conventionally-treated bednet. The adjustable distance between the gas exit of the DART source and the sample holder (see Figure 2.1) allowed two settings to be examined at various gas flow rates: in contact with one another (▲) and 4 mm apart (×). Set gas temperature was 150 °C in all cases.

The two positions tested were: in contact with the ion source gas nozzle (▲) and 4 mm apart (×) from it. It was observed that when the ion source outlet was in contact with the sample holder, the ion intensity increased with gas flow rate. Conversely, for a source-to-holder distance of 4 mm, the ion intensity showed a downward trend with increased flow rate. It is not clear as to why one of the data points at 1.5 L min^{-1} deviated from the upward trend, but it is possible that this deviation was caused by improper placement of the holder.

The trends seen in Figure 3.4 are supported by computational fluid dynamic (CFD) simulations of the ionization region. When the sample holder is 4 mm away from the DART gas nozzle, the reactive gas stream collides into the peripheral regions of the

MACOR sample opening, deflecting some of the reactive gas plume away from the bednet (Figure 3.5).

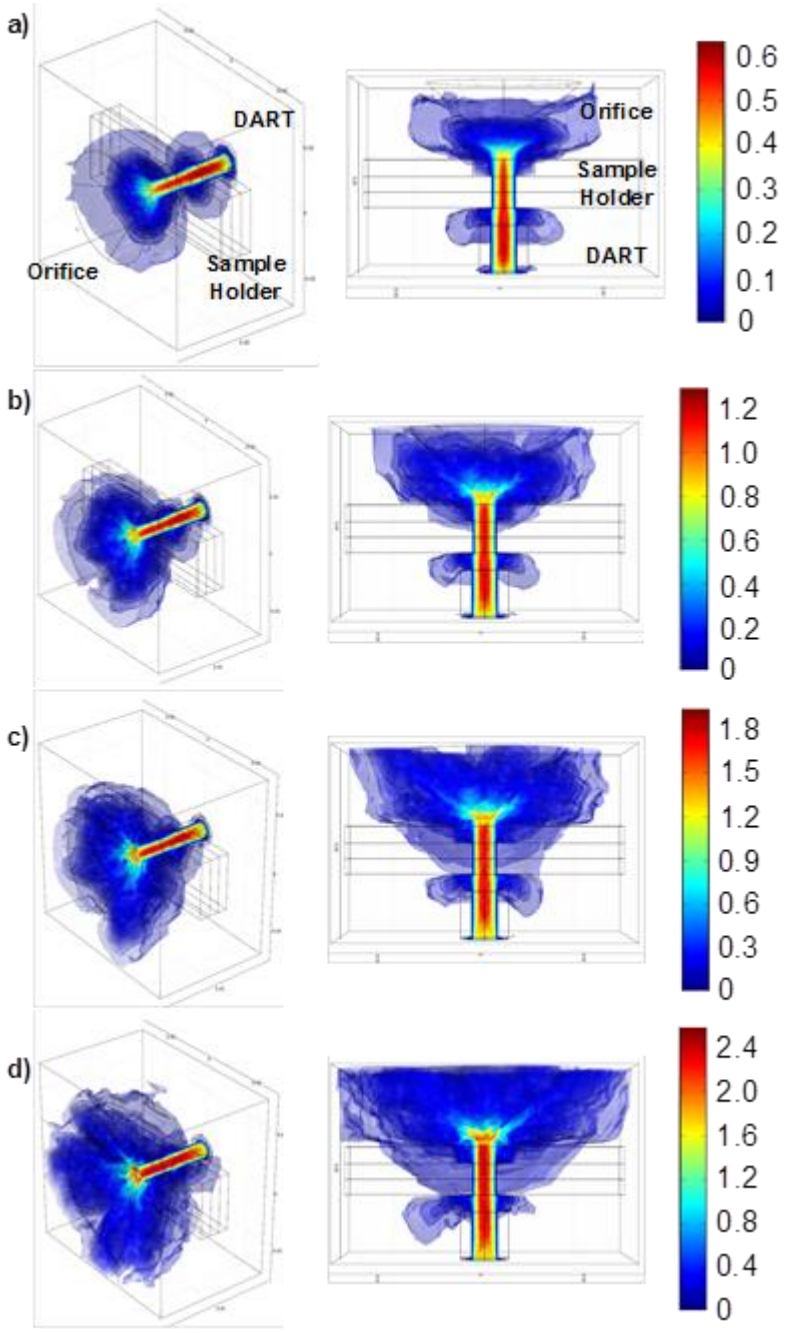

Figure 3.5. CFD simulations at a) 0.5, b) 1.0, c) 1.5 and d) 2.0 L min^{-1} He at 150 ºC when the DART gas nozzle is positioned 4 mm away from the sample holder. The images on the left show a 3D perspective of the system, the middle images show the gas flow from above, and the heat map scales on the right are the gas velocities in m s^{-1}.

When the gas flow rate is set to 0.5 and 1.0 L min^{-1} (Figure 3.5a and b, respectively), the deflection is fairly homogenous with respect to the sample hole opening. As the gas flow rate increases to 1.5 and 2.0 L min^{-1} (Fig. 3.5c and d, respectively), the deflected gas travels further away from the sample entrance and in more erratic directions. Although the overall gas velocity remains high, the presence of fewer reactive species passing through the net may account for the lower intensity observed as the gas flow rate is increased in this configuration. Conversely, when the DART gas nozzle is directly in contact with the sample holder opening, the high velocity reactive gas is forced through the bednet without gas deflection (Figure 3.6). The overall gas velocities are very similar to those in the previous configuration, but the presence of more reactive species hydrodynamically focused through the net may account for the higher experimental sensitivity observed.

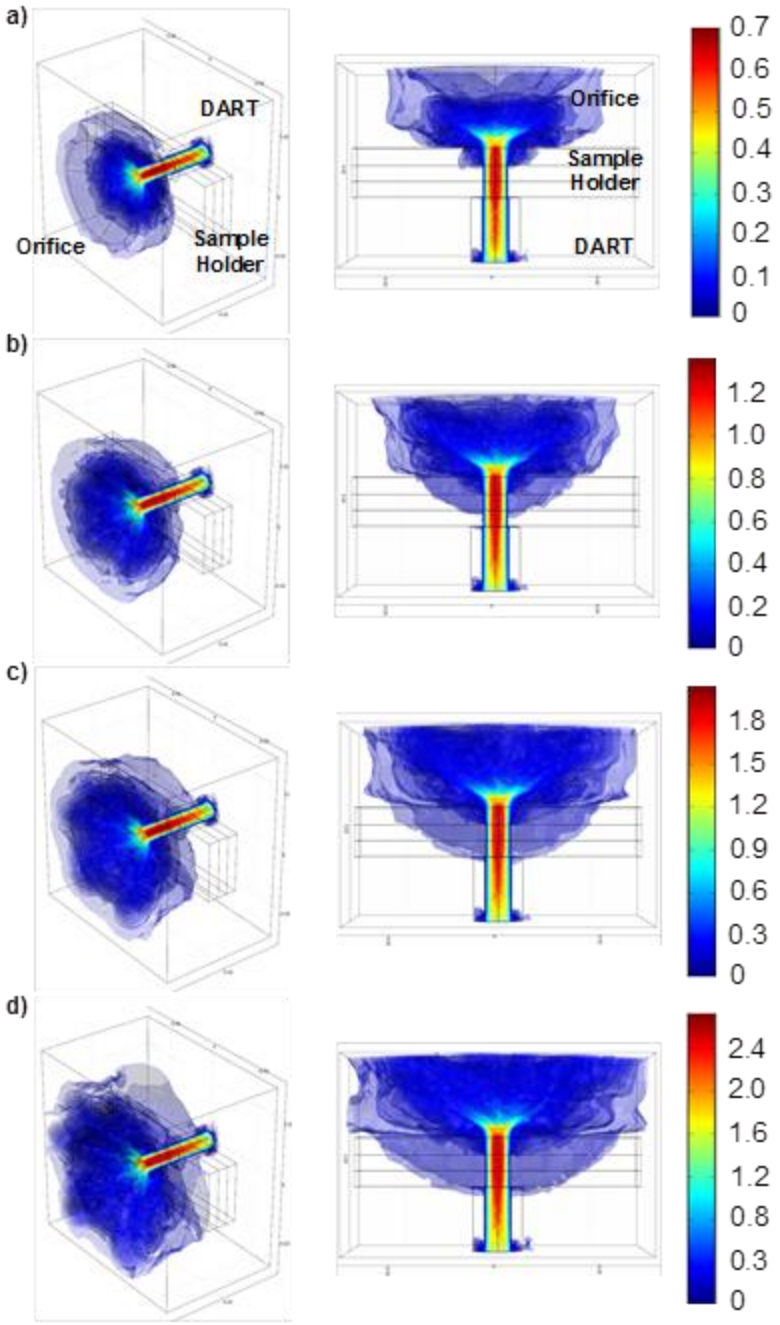

Figure 3.6. CFD simulations at a) 0.5, b) 1.0, c) 1.5 and d) 2.0 L min^{-1} He at 150 ºC when the DART gas nozzle is positioned in contact with sample holder. The images on the left show a 3D perspective of the system, the middle images show the gas flow from above, and the heat map scales on the right are the gas velocities in m s^{-1}.

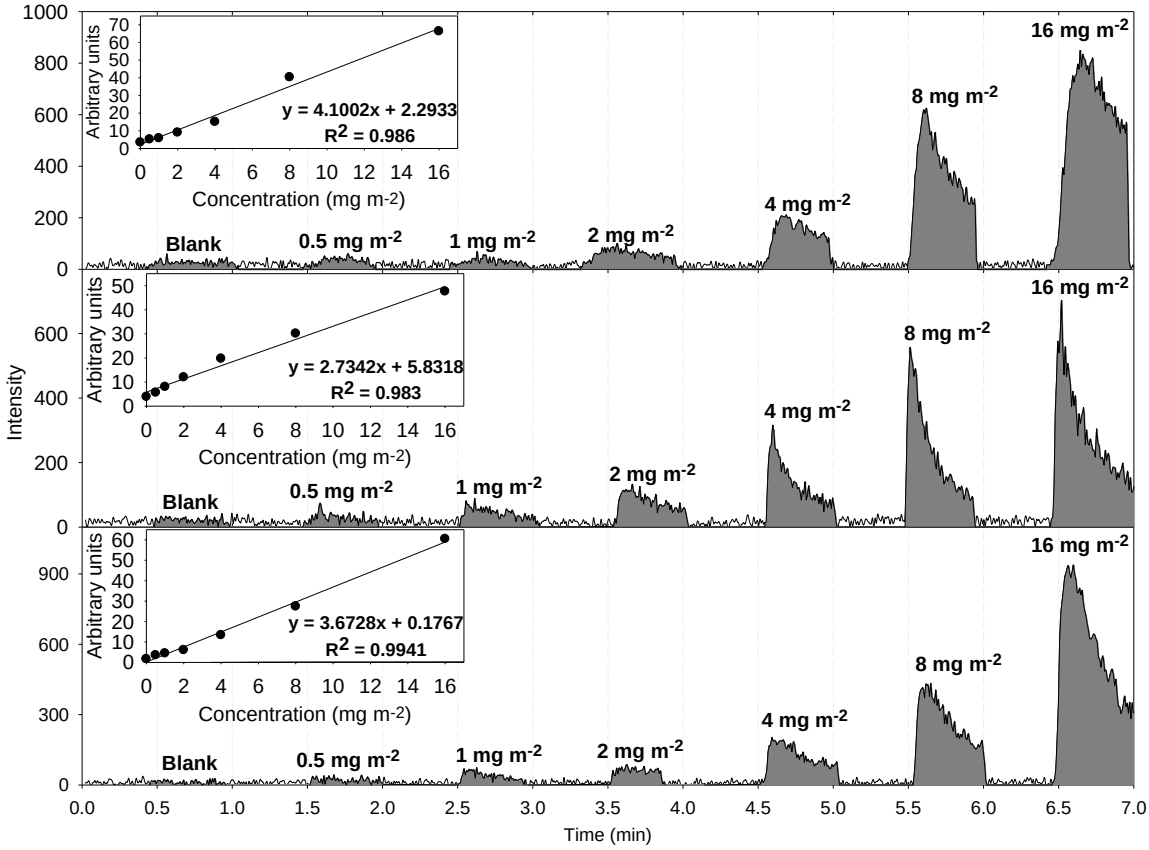

Figure 3.7. Extracted ion chronograms for the TM-DART analysis of bednets coated with increasing levels of deltamethrin using the custom-made sample holder. Experiments were performed using He (0.5 L min^{-1} (top) and 2.0 L min^{-1} (center) at 150 °C) and N_2 (7.0 L min^{-1} at 225 °C (bottom)). Insets show integrated peak areas as a function of bednet insecticide concentration.

Extracted ion chronograms obtained from TM-DART analyses of bednets conventionally treated with increasing levels of deltamethrin are shown in Figure 3.7. The conditions chosen for each analysis were those that overall yielded the highest abundance of the protonated or ammoniated ions. Analysis with He was performed under two sets of conditions: (a) 150 °C, 0.5 L min^{-1}, and 4 mm source-to-holder distance (Figure 3.7, top), and (b) 150 °C, 2.0 L min^{-1} and the source in contact with the holder (Figure 3.7, center). N_2 analysis was performed at 225 °C and 7.0 L min^{-1} with a source-to-holder distance of 4 mm (Figure 3.7, bottom). Bednets treated at various concentration

levels (0–16 mg m^{-2}) were sampled for approximately 30 s. The shaded regions represent the areas integrated for each concentration level, which are plotted in the insets. The observed linearity (R = 0.983 or better) suggests that TM-DART has potential for semi-quantitative determination of pesticides in ITNs, and that levels as low as 0.5 mg m^{-2} (10 ng) of deltamethrin can be detected with either He or N_2 TM-DART.

LLINs manufactured by impregnation with deltamethrin (PermaNet® 2.0) and permethrin (Olyset®) were also investigated to ascertain the feasibility of testing modern bednets. PermaNet® 2.0 nets contain the deltamethrin insecticide mixed in a resin which coats the fibers of the polyester net.

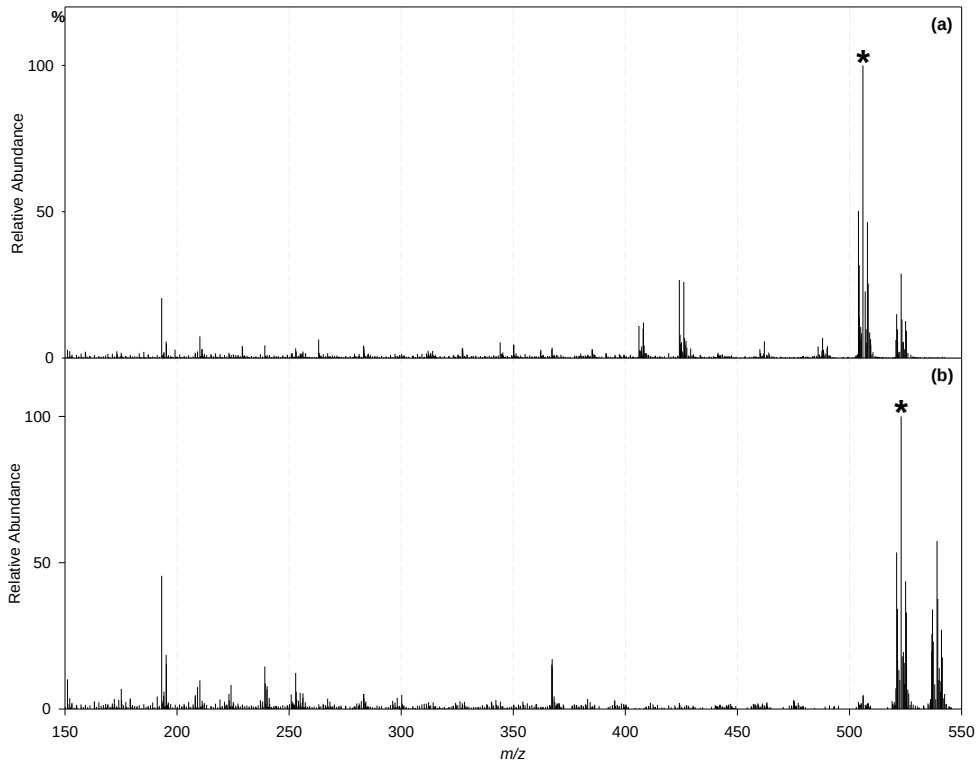

Figure 3.8. He- and N_2-induced TM-DART spectra of a 55 mg m^{-2} deltamethrin-impregnated PermaNet® 2.0 net. (a) Helium spectrum obtained at 150 °C and 2 L min^{-1}; (b) N_2 spectrum obtained at 150 °C and 7 L min^{-1}. Asterisks indicate the $[M+H]^+$ and $[M+NH_4]^+$ for the He and N_2 spectra, respectively.

Figure 3.8 shows (a) a He spectrum at 2 L min^{-1} and (b) a N_2 spectrum at 7 L min^{-1} of a PermaNet containing 55 mg deltamethrin m^{-2}. Olyset® nets, which incorporate permethrin within the fibers of a polyethylene net, allow the migration of insecticide to the surface of the fiber over time, maintaining an approximately constant surface concentration. Figure 3.9 shows (a) He and (b) N_2 TM-DART spectra of an Olyset® net, containing 1000 mg permethrin m^{-2}.

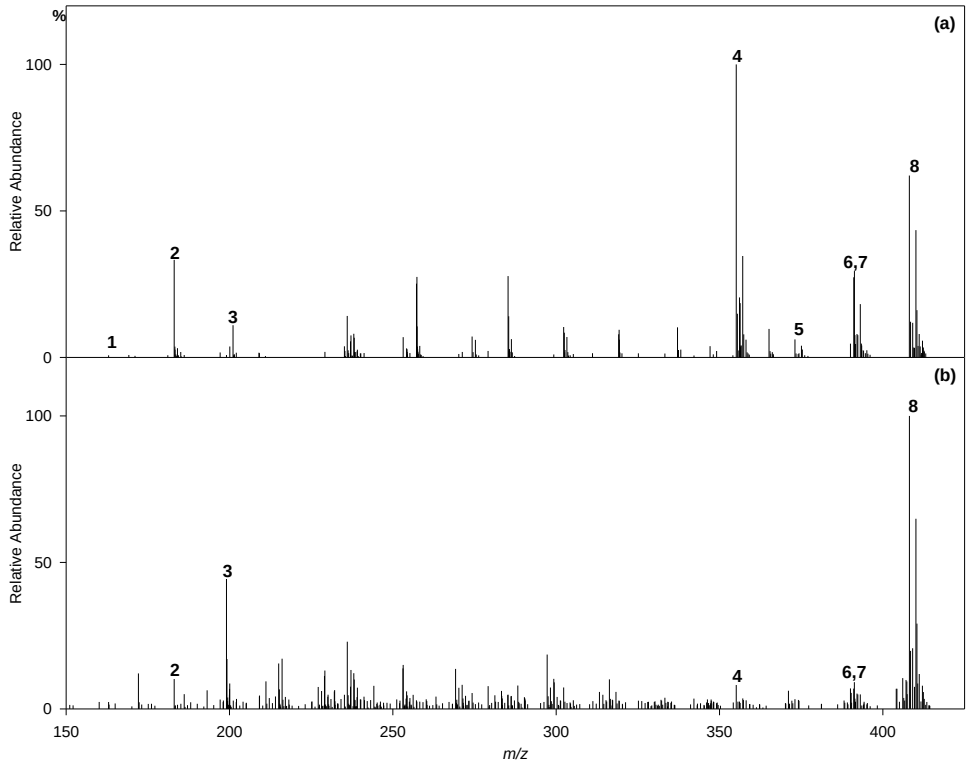

Figure 3.9. He- and N_2-induced TM-DART spectra of a 1000 mg m^{-2} permethrin-impregnated Olyset® net. (a) He spectrum obtained at 150 °C and 2 L min^{-1}; (b) N_2 spectrum obtained at 150 °C and 7 L min^{-1}. Spectral peak assignments are consistent with those identified in Figure 2.3 and listed in Table 2.2.

The labeled ions match those previously identified in Figure 3.2 and Table 3.2. The DART spectra of LLINs illustrated in Figures 3.8 and 3.9 show good agreement with

spectra obtained from conventionally-treated nets, despite the differences in the manufacturing process.

Whereas DART involves ionization mechanisms akin to atmospheric pressure chemical ionization resulting in protonation and adduction of the insecticide, electrospray mechanisms are known to prevail in DESI.[8] Previous LC-ESI-MS studies of pyrethroids, including deltamethrin and permethrin, demonstrated that the primary ESI pathway was cation adduction.[56, 57] In particular, ammonium adducts were reported to dominate the LC-MS spectra, and only a minimal amount of protonated species was observed. A number of TM-DESI solvents (e.g., methanol, acetonitrile, water–methanol solutions) were tested in the present study. Not surprisingly, the largest and most reproducible TM-DESI responses were observed when the electrospray solvent was doped with ammonium acetate to facilitate cation adduction, and ultimately gas-phase ionization. This method of solvent doping, known as reactive DESI, takes advantage of the unique chemistry that exists when a desorbed neutral analyte is sequestered within a charged electrospray droplet containing reactive species.[14, 58, 59]

TM-DESI analyses were conducted on a linear ion trap (LIT) mass spectrometer capable of performing multiple stages of tandem mass spectrometry. Thus, a consecutive reaction monitoring (CRM) strategy was developed to increase the specificity of deltamethrin detection. Figure 3.10 depicts an extracted ion chronogram for the TM-DESI analysis of a polyester bednet coated with 16 mg deltamethrin m^{-2}.

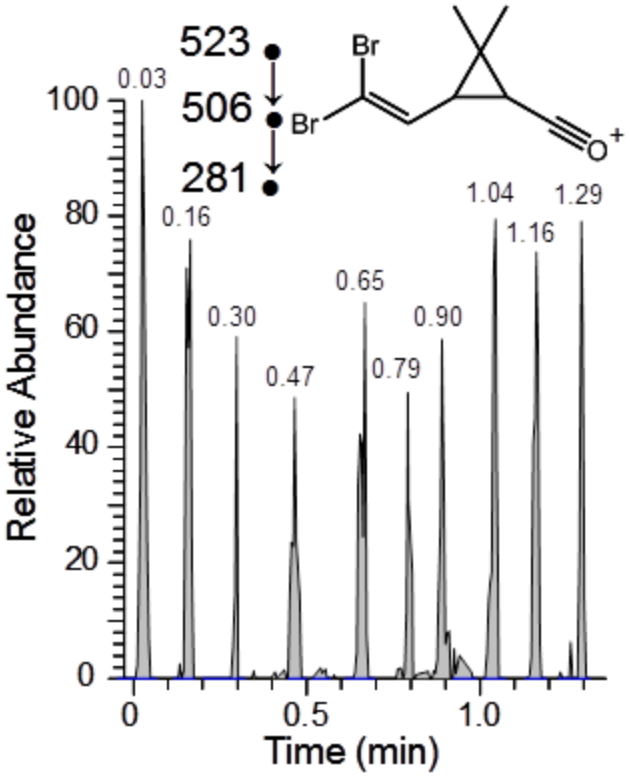

Figure 3.10. Extracted ion chronogram for the TM-DESI analysis of a polyester bednet conventionally treated with 16 mg deltamethrin m^{-2}. The consecutively monitored reaction encompassed CID of the most abundant isotope of the ammonium adduct (*m/z* 523) to the protonated species of *m/z* 506. Isolation and further CID generated the MS^3 product ion of *m/z* 281, whose proposed structure is shown in the inset. Since the unit cell dimension of the bednet (2 mm) is greater than the TM-DESI sampling diameter (~1 mm), each strand of the bednet was clearly discernible in the chronogram.

The CRM method entailed collisional induced dissociation (CID) of the most abundant ammonium adduct isotope (*m/z* 523) to generate protonated deltamethrin ions (*m/z* 506). Isolation followed by a second stage of CID generated the MS^3 product ion of *m/z* 281, whose proposed structure is shown in the inset. Analysis of both coated bednets and LLINs produced reliable detections for deltamethrin at concentrations greater than or equal to 8 mg m^{-2}. Deltamethrin was not detected on polyester bednets with lower concentrations, thereby indicating that TM-DART was more sensitive under the

conditions tested here. However, further optimization of experimental variables may allow lower TM-DESI MS detection limits.

The spatial-scanning capabilities of the TM-DESI ionization source made this technique a useful complement to the previously discussed TM-DART results. As with all TM-DESI experiments, the characteristics of the mesh have an important influence on the transmission of the electrospray and ultimately on the observed mass spectrum.[60] In the particular application explored here, the open space of the coated polyester bednet was on the order of 2 mm, with a strand diameter of approximately 250 μm. This resulted in a unit cell dimension of approximately 2500 μm 2500 μm, if calculated from the mesh open space plus twice the strand diameter. With the electrospray flow rate, nebulizing gas pressure, and electrospray tip-to-sample distance used in the TM-DESI MS experiments presented here, an effective sampling diameter of approximately 1 mm was achieved.[60] Since the unit cell dimension was greater than the sampling diameter, it was possible for the sampling jet to pass entirely through a unit cell. Consequently, each strand of the polyester bednet could be interrogated independently if the scan rate was sufficiently low. Experimentally, a surface scan rate of 250 μm s^{-1} was observed to suffice.

The extracted ion chronogram in Figure 3.10 clearly shows that deltamethrin was detected at approximately 8 s (0.13 min) intervals during the TM-DESI bednet scan. At the specified scan rate, this time interval is equivalent to 2000 μm between peak maxima. These results are in accordance with the measured bednet unit cell dimensions. While no further work to quantify deltamethrin *via* external calibration or through the inclusion of an internal standard was performed, the intensities observed in Figure 3.10 suggest that

the distribution of deltamethrin on the bednet fibers is reasonably consistent. Additional work utilizing a 2D scanning device to compose a chemical image of an entire bednet section would provide further confirmation.[60, 61]

While the difference between the unit cell dimension and sampling diameter facilitated investigation of the individual bednet strands, it also resulted in higher limits of detection since at any given sampling time a relatively small portion of the surface area was exposed to the electrospray. Therefore, additional experiments were performed to assess a new aspect of TM-DESI; one in which a multi-layer folded bednet sample was interrogated with the intention of increasing the observed response. In this case, samples were constructed of one, two, three, four and five layers of bednet material, offset in such a way that the top layer of strands occupied the open space of the mesh layer beneath it.

The resulting extracted ion chronograms for the multi-layer samples no longer contained completely resolved strands. Instead, overlapping contributions from the various strands composing the different layers were observed (Figure 3.11).

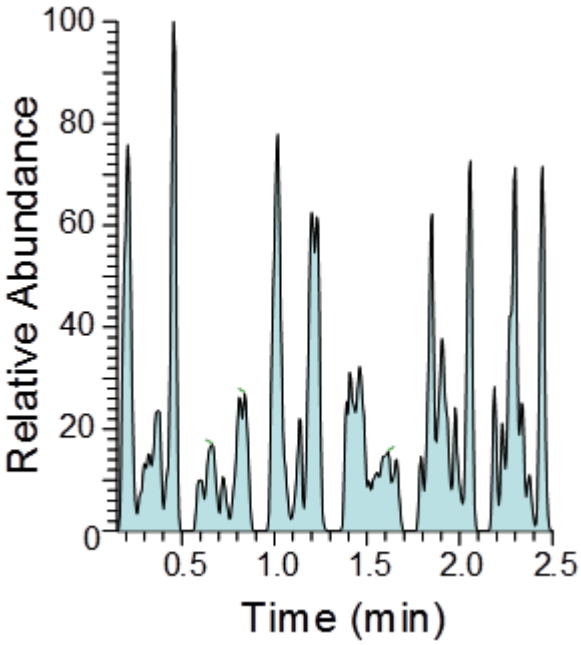

Figure 3.11. TM-DESI MS analysis of a sample composed of three offset layers of a conventionally-treated bednet coated with 16 mg m^{-2} of deltamethrin. Responses for individual strands that were observed in the single-layer sample are no longer observed; however, the greater sample density results in increased response relative to a single-layer sample.

The observed ion intensity for the two- and three-layer samples was higher than for the single layer one. In contrast, deltamethrin was not detected on the four- and five-layer samples, even though the total surface area and effective analyte concentration were larger. These results suggest two important conclusions: (1) it is possible to improve the TM-DESI MS detection limit by utilizing a multilayer sample to introduce more analyte within the electrospray sampling diameter, and (2) that the increase in sensitivity is ultimately limited by the ability of the electrospray to be efficiently transmitted through the sample. Therefore, as noted previously in the analysis of single layer materials,[60] a balance between sample surface area and electrospray transmission must be struck for successful multi-layer TM-DESI MS analyses.

CHAPTER 4

CONCLUSIONS

The results reported here demonstrate TM-DART as an alternative sampling strategy versus traditional methods of probing sample surfaces for DART MS analysis, with particularly interesting application to the analysis of insecticide-treated bednets. The cavity of the custom-made holder creates an ion tunneling effect directly affecting the spectral appearance, following changes in metastable gas temperature and flow rate, and the distance between the gas outlet and the sample being analyzed. Computational fluid dynamic simulations confirmed this effect by illustrating a directed flow of gas transmitting desorbed analyte ions through the sampled mesh and into the MS orifice. Reproducible, quick, and easy mounting/dismounting of the sample holder assembly to a fixed position within the ionization region allows a systematic approach to analyzing ITN samples, providing highly selective semi-quantitative analysis capabilities with throughputs of 60+ samples per hour. Reactive TM-DESI results indicate it as a complementary technique to TM-DART analysis of ITNs. Its ability to analyze one fiber at a time allows the spatial distribution of the insecticide to be evaluated. The ability of performing rapid screening analysis favorably compares TM ambient MS methods against more comprehensive, but slower, chromatographic approaches requiring bednet solvent extraction.

APPENDIX A

ADDITIONAL RESEARCH

The following provides information regarding additional research conducted collaboratively by J.J. Pérez during his time within the research program. J.J. Pérez contributed significantly in both sample preparation and LC-MS method development procedures described in the resulting published research article.[62]

A.1. Abstract

RATIONALE: Cystic fibrosis related diabetes (CFRD) is an important complication of cystic fibrosis (CF) because it causes acceleration in the decline in lung function. Monitoring concentrations of key metabolites such as glucose in airway lining fluid is necessary for improving our understanding of the biochemical mechanisms linking diabetes and CF. Targeted-metabolomic strategies for glucose quantitation in exhaled breath condensate (EBC) from healthy individuals are presented.

METHODS: Three different electrospray ionization mass spectrometry (ESI-MS)-based methods were developed for EBC sample interrogation and glucose quantitation without derivatization. Two methods utilized ultra-high-performance liquid chromatography (UHPLC) coupled to either time-of-flight (TOF) MS or triple quadrupole (QqQ) tandem MS (MS/MS). A third approach involved direct-infusion traveling wave ion mobility spectrometry (TWIMS) with TOFMS detection. UHPLC/QqQ-MS/MS was used for urea quantitation as the EBC dilution marker. Matrix effects were mitigated using isotopically labeled glucose and urea as internal standards.

RESULTS: All the developed methods allowed glucose and urea quantitation in EBC with high accuracy and precision. The UHPLC/TOF-MS and UHPLC/QqQ-MS/MS

methods provided similar analytical figures of merit. UHPLC/QqQMS/MS provided the highest sensitivity and the lowest limit of detection (LOD) of 1.5 nM in EBC for both glucose and urea. The TWIMS-TOF-MS-based method provided the highest sample throughput capability; however, the glucose LOD was ~3-fold higher than with the two chromatographic methods.

CONCLUSIONS: Mass spectrometric methods for the quantitative analysis of trace EBC glucose levels are reported and compared for the first time. The analytical figures of merit demonstrate the applicability of these methods to metabolite analysis of airway samples for CF and CFRD research.

A.2. Published Article Reference

Monge, M.E.; Pérez, J.J.; Dwivedi, P.; Zhou, M.; McCarty, N.A.; Stecenko, A.A.; Fernández, F.M. "Ion mobility and liquid chromatography/mass spectrometry strategies for exhaled breath condensate glucose quantitation in cystic fibrosis studies." *Rapid Communications in Mass Spectrometry*, 2013, 27, 2263–2271.[62]

REFERENCES

1. J. J. Perez, G. A. Harris, J. E. Chipuk, J. S. Brodbelt, M. D. Green, C. Y. Hampton and F. M. Fernandez, *Analyst*, 2010, 135, 712-719.

2. Z. Takats, J. M. Wiseman, B. Gologan and R. G. Cooks, *Science*, 2004, 306, 471-473.

3. J. A. Laramee, H. D. Durst, R. B. Cody and J. M. Nilles, *Abstracts of Papers of the American Chemical Society*, 2005, 230, U313-U313.

4. H. Chen, G. Gamez and R. Zenobi, *Journal of the American Society for Mass Spectrometry*, 2009, 20, 1947-1963.

5. G. A. Harris, A. S. Galhena and F. M. Fernandez, *Analytical Chemistry*, 2011, 83, 4508-4538.

6. G. A. Harris, L. Nyadong and F. M. Fernandez, *Analyst*, 2008, 133, 1297-1301.

7. G. J. Van Berkel, S. P. Pasilis and O. Ovchinnikova, *Journal of Mass Spectrometry*, 2008, 43, 1161-1180.

8. A. Venter, M. Nefliu and R. G. Cooks, *Trac-Trends in Analytical Chemistry*, 2008, 27, 284-290.

9. D. J. Weston, *Analyst*, 2010, 135, 661-668.

10. J. H. Gross, *Analytical and Bioanalytical Chemistry*, 2014, 406, 63-80.

11. R. B. Cody, *Analytical Chemistry*, 2009, 81, 1101-1107.

12. K. Hiraoka, S. Fujimaki, S. Kambara, H. Furuya and S. Okazaki, *Rapid Communications in Mass Spectrometry*, 2004, 18, 2323-2330.

13. L. Song, A. B. Dykstra, H. Yao and J. E. Bartmess, *Journal of the American Society for Mass Spectrometry*, 2009, 20, 42-50.

14. Z. Takats, J. M. Wiseman and R. G. Cooks, *Journal of Mass Spectrometry*, 2005, 40, 1261-1275.

15. J. P. Williams, V. J. Patel, R. Holland and J. H. Scrivens, *Rapid Communications in Mass Spectrometry*, 2006, 20, 1447-1456.

16. S. S. Zeng, T. Chen, L. Wang and H. B. Qu, *Journal of Pharmaceutical and Biomedical Analysis*, 2013, 76, 87-95.

17. F. M. Fernandez, R. B. Cody, M. D. Green, C. Y. Hampton, R. McGready, S. Sengaloundeth, N. J. White and P. N. Newton, *Chemmedchem*, 2006, 1, 702-+.

18. P. N. Newton, F. M. Fernandez, A. Plancon, D. C. Mildenhall, M. D. Green, L. Ziyong, E. M. Christophel, S. Phanouvong, S. Howells, E. McIntosh, P. Laurin, N. Blum, C. Y. Hampton, K. Faure, L. Nyadong, C. W. R. Soong, B. Santoso, W. Zhiguang, J. Newton and K. Palmer, *Plos Medicine*, 2008, 5, 209-219.

19. L. Nyadong, G. A. Harris, S. Balayssac, A. S. Galhena, M. Malet-Martino, R. Martino, R. M. Parry, M. D. M. Wang, F. M. Fernandez and V. Gilard, *Analytical Chemistry*, 2009, 81, 4803-4812.

20. S. Sengaloundeth, M. D. Green, F. M. Fernandez, O. Manolin, K. Phommavong, V. Insixiengmay, C. Y. Hampton, L. Nyadong, D. C. Mildenhall, D. Hostetler, L. Khounsaknalath, L. Vongsack, S. Phompida, V. Vanisaveth, L. Syhakhang and P. N. Newton, *Malaria Journal*, 2009, 8.

21. J. M. Nilles, T. R. Connell and H. D. Durst, *Analytical Chemistry*, 2009, 81, 6744-6749.

22. F. Rowell, J. Seviour, A. Y. Lim, C. G. Elumbaring-Salazar, J. Loke and J. Ma, *Forensic Science International*, 2012, 221, 84-91.

23. G. Morlock and Y. Ueda, *Journal of Chromatography A*, 2007, 1143, 243-251.

24. K. Kpegba, T. Spadaro, R. B. Cody, N. Nesnas and J. A. Olson, *Analytical Chemistry*, 2007, 79, 5479-5483.

25. O. P. Haefliger and N. Jeckelmann, *Rapid Communications in Mass Spectrometry*, 2007, 21, 1361-1366.

26. S. J. B. Dunham, P. D. Hooker and R. M. Hyde, *Forensic Science International*, 2012, 223, 241-244.

27. S. Houlgrave, G. M. LaPorte, J. C. Stephens and J. L. Wilson, *Journal of Forensic Sciences*, 2013, 58, 813-821.

28. R. W. Jones, R. B. Cody and J. F. McClelland, *Journal of Forensic Sciences*, 2006, 51, 915-918.

29. A. D. Lesiak, R. A. Musah, R. B. Cody, M. A. Domin, A. J. Dane and J. R. E. Shepard, *Analyst*, 2013, 138, 3424-3432.

30. R. A. Musah, R. B. Cody, A. J. Dane, A. L. Vuong and J. R. E. Shepard, *Rapid Communications in Mass Spectrometry*, 2012, 26, 1039-1046.

31. R. A. Musah, M. A. Domin, R. B. Cody, A. D. Lesiak, A. J. Dane and J. R. E. Shepard, *Rapid Communications in Mass Spectrometry*, 2012, 26, 2335-2342.

32. R. A. Musah, M. A. Domin, M. A. Walling and J. R. E. Shepard, *Rapid Communications in Mass Spectrometry*, 2012, 26, 1109-1114.

33. R. R. Steiner and R. L. Larson, *Journal of Forensic Sciences*, 2009, 54, 617-622.

34. C. Y. Pierce, J. R. Barr, R. B. Cody, R. F. Massung, A. R. Woolfitt, H. Moura, H. A. Thompson and F. M. Fernandez, *Chemical Communications*, 2007, DOI: 10.1039/b613200f, 807-809.

35. E. Jagerdeo and M. Abdel-Rehim, *Journal of the American Society for Mass Spectrometry*, 2009, 20, 891-899.

36. C. M. Jones and F. M. Fernandez, *Rapid Communications in Mass Spectrometry*, 2013, 27, 1311-1318.

37. Y. P. Zhao, M. Lam, D. L. Wu and R. Mak, *Rapid Communications in Mass Spectrometry*, 2008, 22, 3217-3224.

38. M. Zhou, W. Guan, L. D. Walker, R. Mezencev, B. B. Benigno, A. Gray, F. M. Fernandez and J. F. McDonald, *Cancer Epidemiology Biomarkers & Prevention*, 2010, 19, 2262-2271.

39. M. Zhou, J. F. McDonald and F. M. Fernandez, *Journal of the American Society for Mass Spectrometry*, 2010, 21, 68-75.

40. A. H. Grange, *Rapid Communications in Mass Spectrometry*, 2013, 27, 305-318.

41. M. Haunschmidt, W. Buchberger, C. W. Klampfl and R. Hertsens, *Analytical Methods*, 2011, 3, 99-104.

42. E. S. Chernetsova and G. E. Morlock, *International Journal of Mass Spectrometry*, 2012, 314, 22-32.

43. D. Saang'onyo, G. Selby and D. L. Smith, *Analytical Methods*, 2012, 4, 3460-3465.

44. D. S. Saang'onyo and D. L. Smith, *Rapid Communications in Mass Spectrometry*, 2012, 26, 385-391.

45. G. A. Harris and F. M. Fernandez, *Analytical Chemistry*, 2009, 81, 322-329.

46. W. Eberherr, W. Buchberger, R. Hertsens and C. W. Klampfl, *Analytical Chemistry*, 2010, 82, 5792-5796.

47. C. L. Chang, G. G. Xu, Y. Bai, C. S. Zhang, X. J. Li, M. Li, Y. Liu and H. W. Liu, *Analytical Chemistry*, 2013, 85, 170-176.

48. www.ionsense.com.

49. J. E. Chipuk and J. S. Brodbelt, *Journal of the American Society for Mass Spectrometry*, 2008, 19, 1612-1620.

50. T. E. Erlanger, A. A. Enayati, J. Hemingway, H. Mshinda, A. Tami and C. Lengeler, *Medical and Veterinary Entomology*, 2004, 18, 153-160.

51. C. Lengeler, *Bulletin of the World Health Organization*, 2004, 82, 84-84.

52. A. Tami, G. Mubyazi, A. Talbert, H. Mshinda, S. Duchon and C. Lengeler, *Malaria Journal*, 2004, 3.

53. J. E. Gimnig, K. A. Lindblade, D. L. Mount, F. K. Atieli, S. Crawford, A. Wolkon, W. A. Hawley and E. M. Dotson, *Tropical Medicine & International Health*, 2005, 10, 1022-1029.

54. A. Kroeger, O. Skovmand, Q. C. Phan and D. T. Boewono, *Transactions of the Royal Society of Tropical Medicine and Hygiene*, 2004, 98, 152-155.

55. M. D. Green, F. Atieli and M. Akogbeto, *Tropical Medicine & International Health*, 2009, 14, 381-388.

56. M. D. Gil-Garcia, D. Barranco-Martinez, M. Martinez-Galera and P. Parrilla-Vazquez, *Rapid Communications in Mass Spectrometry*, 2006, 20, 2395-2403.

57. D. Zimmer, C. Philipowski, B. Posner, A. Gnielka, E. Dirr and M. Dorff, *Journal of Aoac International*, 2006, 89, 786-796.

58. G. Huang, H. Chen, X. Zhang, R. G. Cooks and Z. Ouyang, *Analytical Chemistry*, 2007, 79, 8327-8332.

59. L. Nyadong, M. D. Green, V. R. De Jesus, P. N. Newton and F. M. Fernandez, *Analytical Chemistry*, 2007, 79, 2150-2157.

60. J. E. Chipuk and J. S. Brodbelt, *Journal of the American Society for Mass Spectrometry*, 2009, 20, 584-592.

61. D. R. Ifa, N. E. Manicke, A. L. Dill and G. Cooks, *Science*, 2008, 321, 805-805.

62. M. E. Monge, J. J. Perez, P. Dwivedi, M. S. Zhou, N. A. McCarty, A. A. Stecenko and F. M. Fernandez, *Rapid Communications in Mass Spectrometry*, 2013, 27, 2263-2271.